Composite Structures 131 (2015) 90–98

Contents lists available at ScienceDirect

Composite Structures

journal homepage: www.elsevier.com/locate/compstruct

Crush responses of composite cylinder under quasi-static and dynamic loading

Louis N.S. Chiu [a,b], Brian G. Falzon [c], Dong Ruan [d], Shanqing Xu [d], Rodney S. Thomson [b,e], Bernard Chen [a], Wenyi Yan [a,*]

[a] Department of Mechanical and Aerospace Engineering, Monash University, Clayton Campus, Victoria 3800, Australia
[b] Cooperative Research Centre for Advanced Composite Structures, 1/320 Lorimer Street, Port Melbourne, Victoria 3207, Australia
[c] School of Mechanical and Aerospace Engineering, Queen's University Belfast, Belfast BT9 5AH, UK
[d] Faculty of Science, Engineering and Technology, Swinburne University of Technology, John Street, Hawthorn, VIC 3122, Australia
[e] Advanced Composite Structures Australia, 1/320 Lorimer Street, Port Melbourne, Victoria 3207, Australia

ARTICLE INFO

Article history:
Available online 6 May 2015

Keywords:
Composites
Crushing
Strain rate effect
Dynamic
Energy absorption

ABSTRACT

Despite the abundance of studies investigating the performance of composite structures under crush loading, disagreement remains in the literature regarding the effect of increased strain rate on the crush response. This study reports an experimental investigation of the behaviour of a carbon–epoxy composite energy absorber under static and dynamic loading with a strain rate of up to 100 s^{-1}. Consistent damage modes and measured force responses were obtained in samples tested under the same strain rate. The energy absorption was found to be independent of strain rate as the total energy absorption appeared to be largely associated with fibre-dominated fracture, which is independent of strain rate within the studied range. The results from this study are beneficial for the design of energy absorbing structures.

1. Introduction

Interest in energy absorbing structures for crashworthiness applications has been growing due to the increasingly safety-conscious environment in which the aviation industry operates. Design guidelines [1] and standards [2] impose a maximum allowable acceleration envelope experienced by the occupant in a crash. Composite materials have been gaining popularity in aircraft structures due to their superior specific strength and stiffness, corrosion and fatigue resistance. Their complex failure modes [3–5] facilitate a high level of energy dissipation making them suitable for use in energy absorbing structures to meet crash protection requirements. Jackson et al. [6] showed that composite energy absorbing structures can significantly reduce the acceleration experienced by the occupants in a crash environment which would reduce risks and severity of injuries. Hence, the performance of composite structures under crush loading is of great interest.

Performance of energy absorbing structures can be measured through their specific energy absorption (*SEA*), peak force (F_{peak}), steady-state force (F_{SS}) and crush efficiency (*CE*). The energy absorption is area under the force (F) – displacement (x) curve, and is directly related to protective capability. *SEA* is defined as the energy absorption of unit mass (m) of structure (Eq. (1)). Hence, for weight-conscious applications such as aviation, *SEA* is a critical measure of performance.

$$SEA = \frac{energy\ absorbed}{mass\ of\ structure\ consumed} = \frac{\int_{x_{start}}^{x_{end}} F\,dx}{m} \quad (1)$$

F_{peak} is the highest force (hence highest acceleration) experienced during the crush event and is directly related to the potential for injury suffered by the occupants in a crash situation. One of the purposes of the energy absorber is to keep acceleration levels within human tolerance limits. F_{SS} is the mean force during steady-state crushing of the specimen after the consumption of the trigger and the passing of peak force, and is a good indicator of the overall energy absorption capability of the structure. *CE* [7] (Eq. (2)) is the ratio between F_{SS} and F_{peak} (Eq. (2)) and is indicative of the nature of the crush response.

$$CE = \frac{F_{SS}}{F_{peak}} \quad (2)$$

A catastrophic failure is characterised by a high peak force as well as a low steady-state crushing force, and hence a low crush efficiency.

A wide variety of composite energy absorber configurations have been reported in the literature since the pioneering work by Thornton [8] and Farley [9]. Simple geometries such as circular

* Corresponding author.
E-mail address: wenyi.yan@monash.edu (W. Yan).

http://dx.doi.org/10.1016/j.compstruct.2015.04.057
0263-8223/

tubes [9–12], rectangular tubes [13–15] and flat plates [13,16] have been studied extensively. More complex geometries have also been investigated, including C sections [17,18] and I sections [15]. Triggering has been shown to be an important aspect of energy absorbent structure design, with chamfering on the loading surface being most common [19]. Other trigger mechanisms studied include the tulip [12,20] and ply drop [21]. Some authors have designed the structures so that they are self-triggering, for example, using corrugated [22] or hourglass profiles [20]. Others have evaluated different types of material systems and layup configuration [19,23]. However, most of these experimental data were based on quasi-static testing, despite crushing being a dynamic event. Consequently, the effectiveness of energy absorbers can only be reliably determined once an assessment of possible rate dependence is made.

Currently, there is disagreement in the literature [24] over the effect of intermediate nominal loading rate between 0.1 and 100 s^{-1} on the response of composite structures. Initial tests completed by Thornton [8] suggested rate independence for glass and graphite–epoxy cylindrical tubes. Farley [10] noted that for chamfered cylinders, $[0/\pm\theta]_2$ graphite–epoxy specimens were rate insensitive, but Kevlar–epoxy and $[\pm\theta]_3$ graphite–epoxy specimens displayed increased specific energy absorption (SEA) as the testing speed increased. Palanivelu et al. [7] found the SEA of specimens with a circular cross-section were rate insensitive, whereas those with a square cross-section increased slightly with crush speed. Work done on rectangular tubes by Mamalis et al. [25] has found that both the SEA and peak force of square tubes increased with respect to increasing strain rate. On the other hand, crush testing conducted by Jackson et al. [17] on chamfered C-section found an approximately 10% reduction in SEA for specimens impacted at 8.5 m/s when compared, with those crushed at 20 mm/s. This was confirmed by David et al. [18] who also observed a reduced SEA on dynamically tested C-section specimens with a $[(0/90)_2/0/(90/0)_2]$ layup. Brighton et al. [26] reported a decrease in SEA for chamfered carbon–epoxy tubes with a $[0/90]_4$ layup when the test speed was increased whereas the rate effect for a chamfered 4 ply glass-polypropylene fabric tubes were inconclusive.

A sufficiently large sample size is often required to measure the scatter in the experimental data. Brighton et al. [26] noted that the lack of manufacturing control has a significant effect on the specimen response which leads to possible strain rate effect being hidden within the noise. Unstable collapse of specimens [25] also presented challenges in their measurement due to the presence of high force spikes in the resulting force response. Furthermore, unstable crushing response is also more dependent on any microscopic defects or weak points within the structure, which are random in nature. In order for a conclusion to be drawn with confidence, the observed trend must be compared with the size of the scatter inherent in the experimental results.

This study presents a comparison between the response and damage mechanisms of a tulip triggered composite cylinder subjected to quasi-static and dynamic crush loading with strain rates of up to 100 s^{-1}. Qualitative analysis of the specimens was conducted to identify the damage modes and their propagation through the structure. Quantitative analysis of the force response for each test condition was also completed. The reliability of the results was assessed through analysing the scatter of the measured data.

2. Experimental method

2.1. Specimen design

The specimen is a cylindrical tube with a series of tulip triggers cut into the top surface. The tubes were manufactured using a unidirectional Hexcel HexPly T700/M21 carbon–epoxy prepreg with a $[0/90/0/90]_s$ layup. The tubes were autoclave cured as per manufacturer's specifications. The effect of seams is minimised by placing seams of adjacent plies on opposing sides of the cylinder. After curing, the composite tubes were machined to the geometry specified in Fig. 1.

A tubular geometry was selected to facilitate their testing as free-standing energy absorbers. A circular cross-section also avoids stress concentrations, which leads to a more steady and localised damage progression [19], resulting in a higher energy absorption in comparison with a square or rectangular cross-section. The triangular tulip trigger can achieve a higher steady-state crush load [19] in contrast to hourglass [20], crown and chamfer [27] triggers, leading to increased energy absorption. The increased length of the trigger region helps to spread the force spike in the initial stage of impact and reduce the peak transmitted force. A balanced $[0/90/0/90]_s$ layup was chosen to ensure lateral confinement and support within the orthogonal plies. Jacob et al. [24] noted increased overall energy absorption when fibres parallel to the loading direction were laterally supported, leading to increased fracture of these fibres. Commercially available filament wound tubes were not considered due to a lack of fibres parallel to the loading direction.

2.2. Test method

MIL-STD-1290A [2] sets out that airframes should be designed for at least an 8 m/s vertical speed at impact. NASA [28] conducted drop tests on representative fuselage sections with attached energy absorbers at impact speeds between 7.3 to 11.6 m/s, which correspond to nominal strain rates of between 15 and 23 s^{-1} in these absorbers. These are the likely strain rates experienced in a survivable crash scenario. Hence, the chosen strain rates for this study were 2.1×10^{-4}, 0.2, 30, 60 and 100 s^{-1} to encompass likely strain rates that an energy absorber would be exposed to in the event of a crash. The chosen specimens were tested at a range of different strain rates, as detailed in Table 1, along with the number of specimens associated with each test configuration.

The specimens for the low rate tests (2.1×10^{-4} and 0.2 s^{-1}) rested freely on the lower steel platen while the top steel platen descended on the specimen at the designated speed. The force measurement was recorded directly from the load cell attached to the top platen and the displacement was obtained from the moving crosshead. In contrast, the Instron 8800 VHS machine used for high strain rate tests has a fixed upper platen with an attached load cell. The bottom platen was then driven upwards using a hydraulic ram to crush the specimen in between. The specimen was fixed on the bottom platen with a small amount of adhesive to prevent it from detaching during its acceleration to the desired test speed. The crush stroke was nominally set to 40 mm. The platen then progressed approximately another 20 mm for the hydraulic system to bring the piston and attached platen to a complete stop at the end of the test. This deceleration phase significantly contributed to the variation in the actual test speed.

3. Results and analysis

3.1. Comparison of damage modes

The typical crush progression of a low rate test is shown in Fig. 2. The eight tulip peaks provided trigger points for damage initiation. The sharp tips of the tulip triggers were easily damaged by the loading surface, which created points of initiation where the damage then spread progressively throughout the entire structure. This process maximised the amount of material damaged and

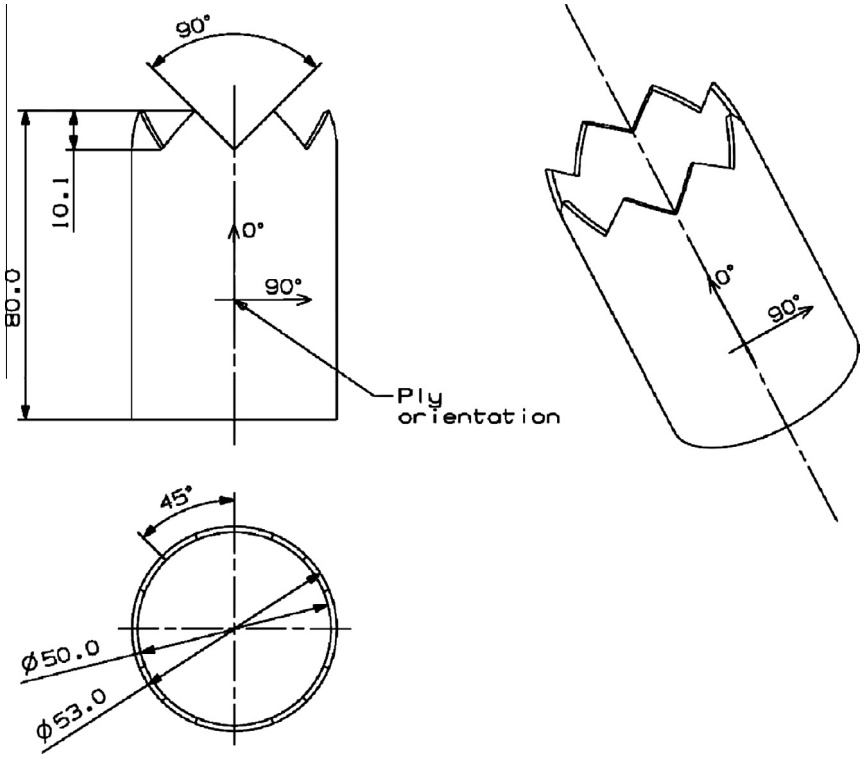

Fig. 1. Test specimen: cylindrical tube topped with tulip triggers.

Table 1
Test conditions.

Testing machine type	Low loading rate		High loading rate		
	Screw-driven		Hydraulic		
Nominal strain rate	2.1×10^{-4} s^{-1}	0.2 s^{-1}	30 s^{-1}	60 s^{-1}	100 s^{-1}
Nominal platen speed	17 μm/s	16 mm/s	2.4 m/s	4.8 m/s	8.0 m/s
Actual test speed	17 μm/s	16 mm/s	2.6–2.0 m/s	5.0–4.0 m/s	8.3–5.5 m/s
Number of specimens	6	6	4	5	7

hence the total energy absorption whilst preventing high peak load at the onset of crushing. Significant delamination occurred throughout the test. The outer-most ply tended to separate from the bulk of the tube, with delamination advancing a significant distance past the crush front. This ply splayed outwards due to the confines of the platen and the inner plies, which also prompts splitting of the ply parallel to the fibre direction. The lengths of these splits are closely related to the amount of delamination experienced by the ply. As splits form in these outer 0° plies, debris falls through the created gaps as evident in Fig. 2(d) (circled). The splits form due to the relatively low matrix strength. Once splitting has occurred, the ply bends and avoids further intralaminar damage caused by subsequent loading.

The crush progression of a typical high rate specimen is shown in Fig. 3. The progression is very similar to those of the low speed tests where damage progressively spread from the trigger tips as the crush stroke increased. The outer-most ply delaminated from the main structure and split along the fibre direction to form petals, which remained relatively intact.

A visual inspection of the damage identified in the post-test examinations of typical low and high rate test specimens is presented in Fig. 4. In both cases, the inner-most ply exhibited similar behaviour as the outer-most ply. The split segments of the outer plies remained relatively intact in contrast to the internal plies (point A in Fig. 4). These outer plies segments formed a funnel-like structure, which trapped debris formed from the disintegration of the internal plies. Due to the confining effects of the outer plies, the internal plies underwent substantial damage that generated a large amount of loosely held debris, regardless of whether they were of 0° or 90° orientation. The damage sustained by the internal plies was also consistent in low and high rate tests. The fibres in the 0° plies tended to break into smaller pieces due to the confining effects of neighbouring plies. The resulting fragments were typically short and wide (point B in Fig. 4). The fibres in the 90° plies, which originally ran the circumference of the tube, tended to split into 3 to 4 segments and form thin tendril-like pieces (point C in Fig. 4). The similarity in the damage progression and the appearance of the resulting debris in the different tests suggest the damage mechanisms are strain rate independent.

The consistent damage modes at different strain rates were also observed at a microscopic level. As shown in Fig. 5, identical damage morphologies were observed in the microscopic laminate cross-sections near the crush front in the low strain rate (0.2 s^{-1}) and the high strain rate (60 s^{-1}) tests.

The major difference between the high and low rate specimens is the distribution of debris at the end of the test. The debris in the low rate test largely remained where it was formed whereas the debris in the high rate tests generally moved towards the centre.

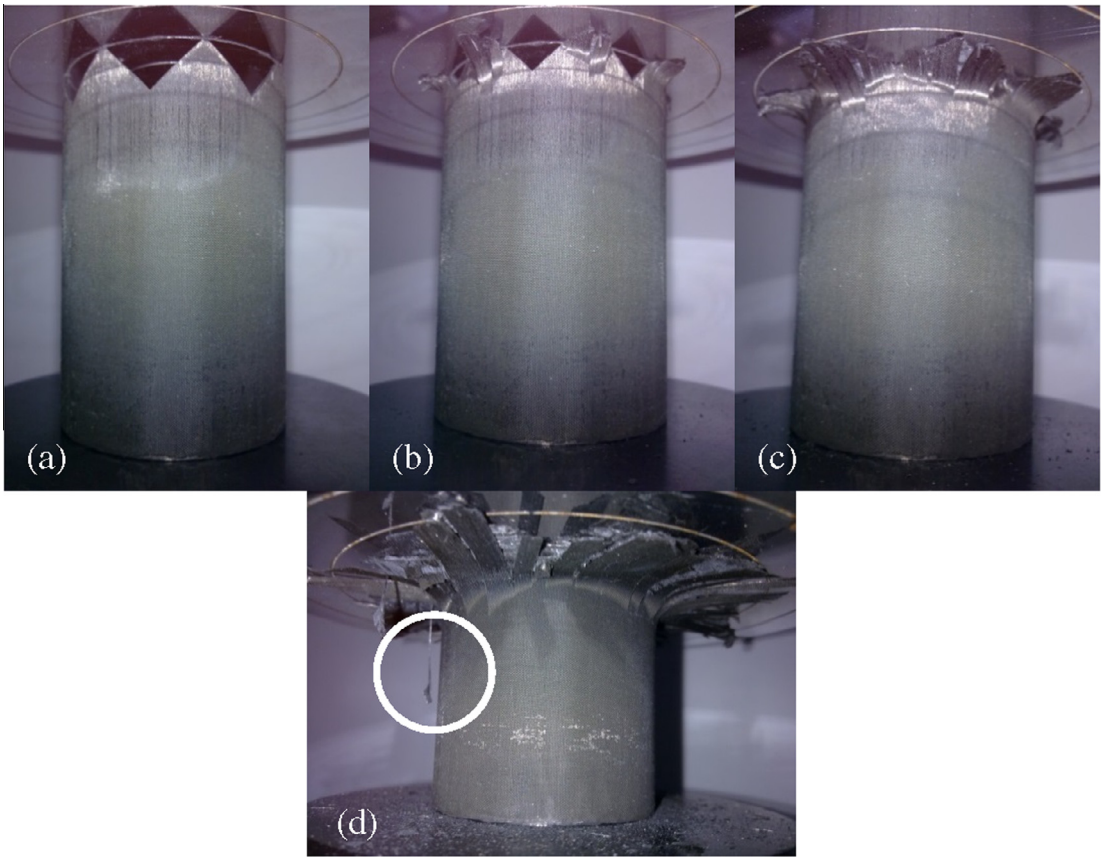

Fig. 2. Typical specimen damage progression when crushed at $2.1 \times 10^{-4}\ s^{-1}$: (a) initial, (b) consumption of trigger region, (c) transition to bulk crushing and (d) steady-state crushing of bulk tube.

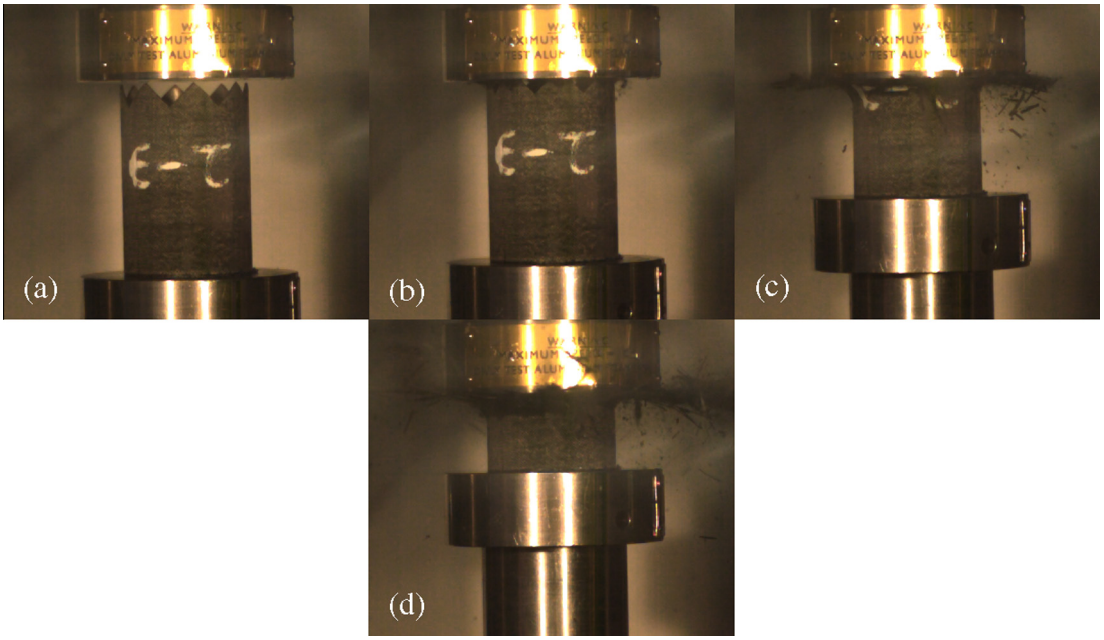

Fig. 3. Typical specimen damage progression when crushed at $60\ s^{-1}$: (a) initial, (b) consumption of trigger region, (c) transition to bulk crushing and (d) steady-state crushing of bulk tube.

This was caused by the outer ply extending past the edge of the platen on the hydraulic testing machine. As the platen advanced, the debris would be scraped from the flexible outer-most ply by the edge of the platen towards the centre of the specimen. However, this did not translate to differences in the force response. It was likely that the debris formation process accounted for most of the energy absorption and subsequent motion of the debris was of little significance.

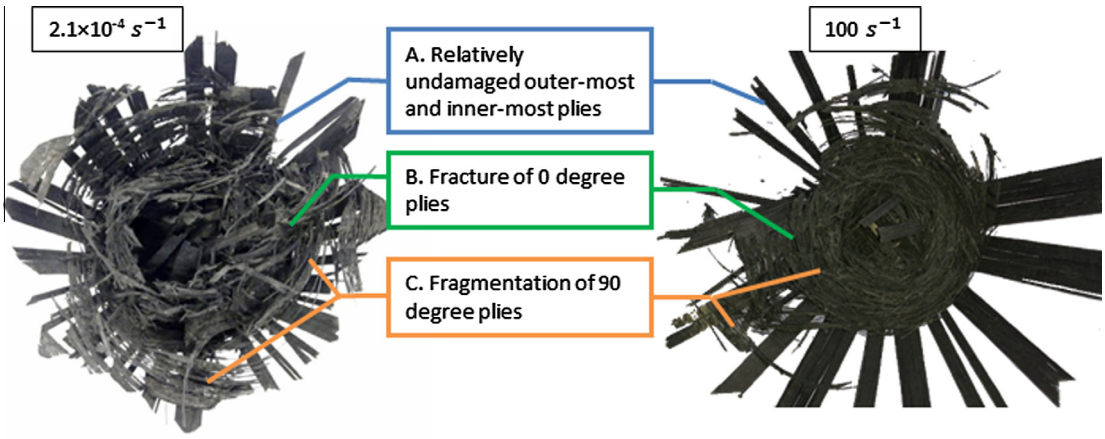

Fig. 4. Comparison of damage distribution between specimens tested at different strain rates.

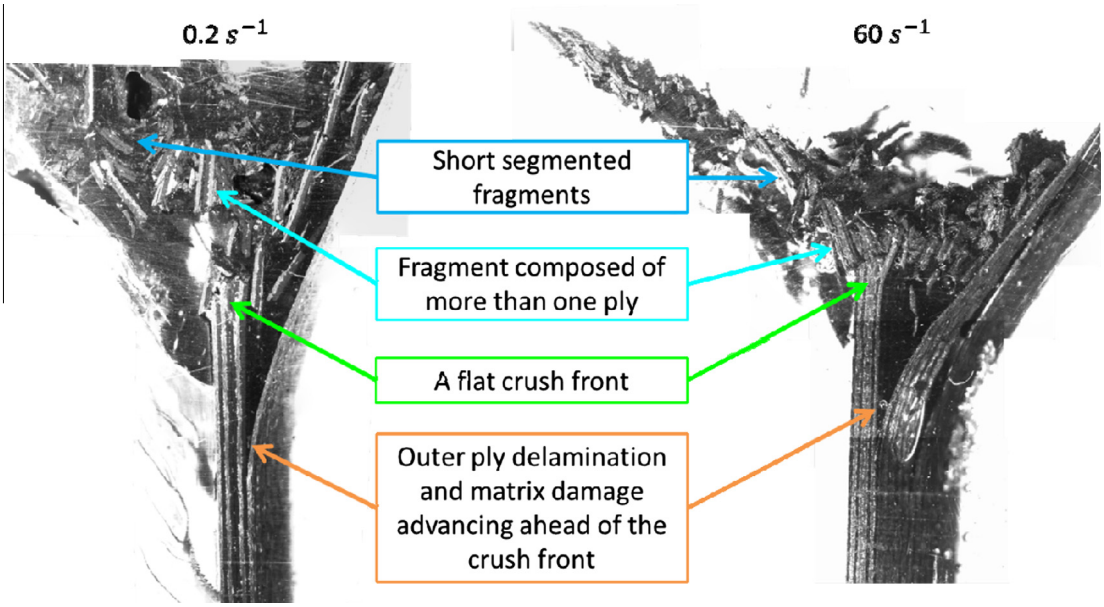

Fig. 5. Microscopic laminate cross-sections near the crush front from the low strain rate ($0.2\,s^{-1}$) and the high strain rate ($60\,s^{-1}$) test showing identical crush front morphology.

The appearance of the debris shed light into the underlying damage mechanism. In the 0° plies, as illustrated in Fig. 6(a), the main form of damage was brittle fibre breakage accompanied by matrix shearing. The majority of loading was borne by the fibres. The longitudinal loading induced hoop stresses in the ply, which were resisted by the matrix between the fibres. These stresses caused failure in the matrix, which destabilised the fibre bundles, making them more susceptible to breakage via bending or shearing.

In comparison, the damage mode of the 90° plies was predominantly shear matrix cracking parallel to the fibre followed by limited breakage of the fibres, as illustrated in Fig. 6(b). The shear cracking was triggered by compressive loading transverse to the ply. After the formation of these rings in the presence of adjacent material, further loading tended to cause a change in the circumference of these rings, inducing fibre breakage due to hoop stresses.

3.2. Comparison of force responses

Fig. 7 shows the force–displacement response recorded for each set of specimens tested at different strain rates. Due to the controlled crushing of the tulip triggers, the first 10 mm of the stroke saw a smooth, linear increase in the reaction force. This is followed by a transition to steady-state crushing of the bulk cylinder where a slight peak was observed. Once the steady-state crushing was established at approximately 15 mm of stroke, the force level remained constant until the end of the test. All response curves took on a similar form. The increasing test rate increased high frequency noise but did not change the shape of the response curve.

Some oscillatory noise can be observed in the force response, particularly in the plateau phase where steady-state crushing occurs. The magnitude of this vibration increased with increasing test rates. The adhesive used to hold the specimen to the platen, as it accelerated to the desired speed, was not sufficiently strong, particularly at the high testing rates. This caused detachment of these specimens to allow them to hit the other platen prematurely. The detachment of the specimens caused the gap in the initial stages of the measured force–displacement curve (Fig. 7(d) and (e)). Removing this gap yielded a force response that was indistinguishable from the force response of specimens that did not experience detachment, hence these results were retained.

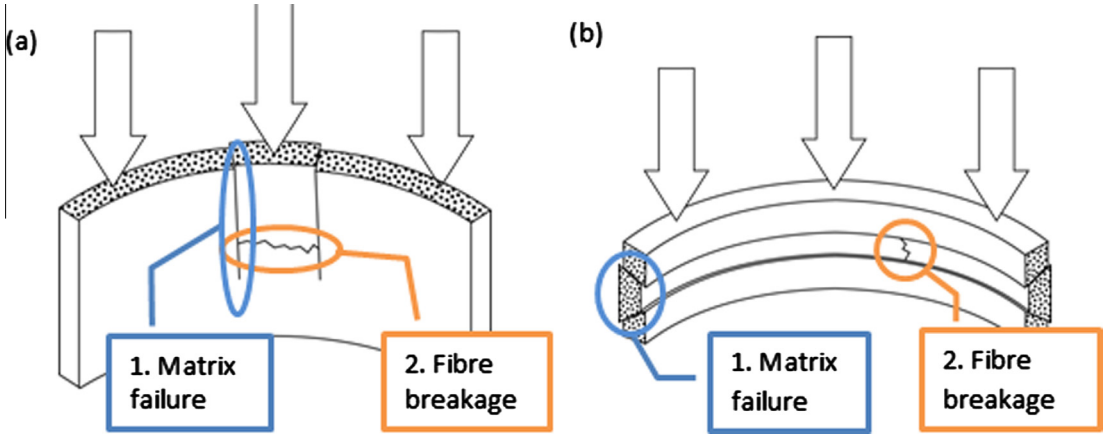

Fig. 6. Damage mechanism in the (a) 0° plies and (b) 90° plies.

3.3. Comparison of SEA, peak forces, steady-state forces and crush efficiencies at different strain rates

The *SEA*, F_{peak}, F_{SS} and *CE* were calculated for each test. Fig. 8 shows the averaged SEA for each strain rate along with its standard deviation. The averaged F_{peak} and F_{SS} are plotted in Fig. 9 for each strain rate. The progression of *CE* is plotted in Fig. 10.

Linear regression was performed to measure the strain rate dependence and the results are shown in Table 2.

Both *SEA* and F_{SS} have small regression gradients and the standard error of these gradients was greater than the magnitude of the gradient. From this, it can be concluded that both *SEA* and F_{SS} are independent of strain rate. The peak force is expected to occur during transition from triggering to steady-state crushing. However, the peak force usually occurred during the steady-state crush region in the high rate tests. This suggests that the increasing oscillatory noise is the cause of the increase in observed F_{peak}. The average amplitude of these high frequency oscillations increased from 4.7 kN for the 2×10^{-4} s^{-1} test to 8.1 kN for the 100 s^{-1} test, which corresponded well to the apparent increase in F_{peak}. Therefore, the increase in F_{peak} with strain rate is likely a result of the vibrations in experimental testing rather than a change in the intrinsic material property. The crush efficiency falls into two distinct groups. The specimens tested on a screw-driven testing machine have higher crush efficiencies than those tested on the hydraulic testing machine. Again, the difference can be attributed to the testing method rather than changes in the underlying material properties.

4. Discussion

4.1. Data reliability

Composite crush structures exhibit complex damage mechanisms, which lead to variability in experimental results. To ensure the validity of the results of the present study, a sample size of between 4 to 7 was used so the scatter in the results of each test configuration can be quantified. In contrast, many authors [7,8,18,25] tested only one specimen per test configuration. The observed damage modes in the present study were also compared against the literature.

The specimens in the present study produced reliable results under the reported testing methods. Pre-test measurement confirmed the consistency in the geometry of specimens. The responses observed between different samples within a batch for each testing condition was also very consistent in terms of the force response as well as the damage pattern. Two typical specimens in the low rate test shown in Fig. 11, demonstrate their similarity. Post-test inspections showed that specimens tested under the same conditions were largely indistinguishable from each other and exhibited the same damage modes.

Correspondingly, the force response data results also exhibited very little scatter. The value of one standard deviation for all measured metrics under every tested strain rate was smaller than 8%. The small scatter observed in both the qualitative and the quantitative measurements indicate the reliability of these results.

The damage observed in this study shares many similarities with results in the literature. Huang et al. [27] observed that unconstrained 0° plies sustained little damage except splitting along the fibre direction, while the 90° plies formed thin strands between the sandwiching 0° plies in quasi-static crushing of chamfered cylinders. The higher resin volume fraction in this material caused it to be less fragmented overall in comparison with the present study. The splaying of the outer ply observed was consistent with observations reported by Jackson et al. [17]. Furthermore, the overall size of individual fragments was also similar. In contrast to the loosely held fragments in the present study, the woven nature of Jackson et al.'s [17] specimen led to the fragments being held together.

4.2. Strain rate independence

The experimental data shows that the material is insensitive to loading rate for intermediate strain rates of up to 100 s^{-1}. Both low and high rate tests yielded specimens with the same damage modes. The force responses also took on the same form and magnitude. The SEA, peak force, steady-state force and crush efficiency did not vary significantly with increasing strain rates. This result contrasts against observations by David et al. [18] and Brighton et al. [26] who observed a significant decrease in SEA for cross-ply laminates at comparable test speeds. In his review, Feraboli also noted that both flat and tubular specimens exhibit a substantial change in SEA beyond 1 m/s [29]. On the other hand, similar strain rate independence was observed by Feraboli [30] for corrugated web with a similar cross-ply layup which was tested at a lower speed of 25 mm/s.

Berthe et al. [31] conducted high rate coupon testing on T700GC/M21 material which showed the shear modulus increased by 40% when the loading rate was increased from 10^{-3} s^{-1} to 88 s^{-1} but no discernible change in the transverse modulus. This suggests

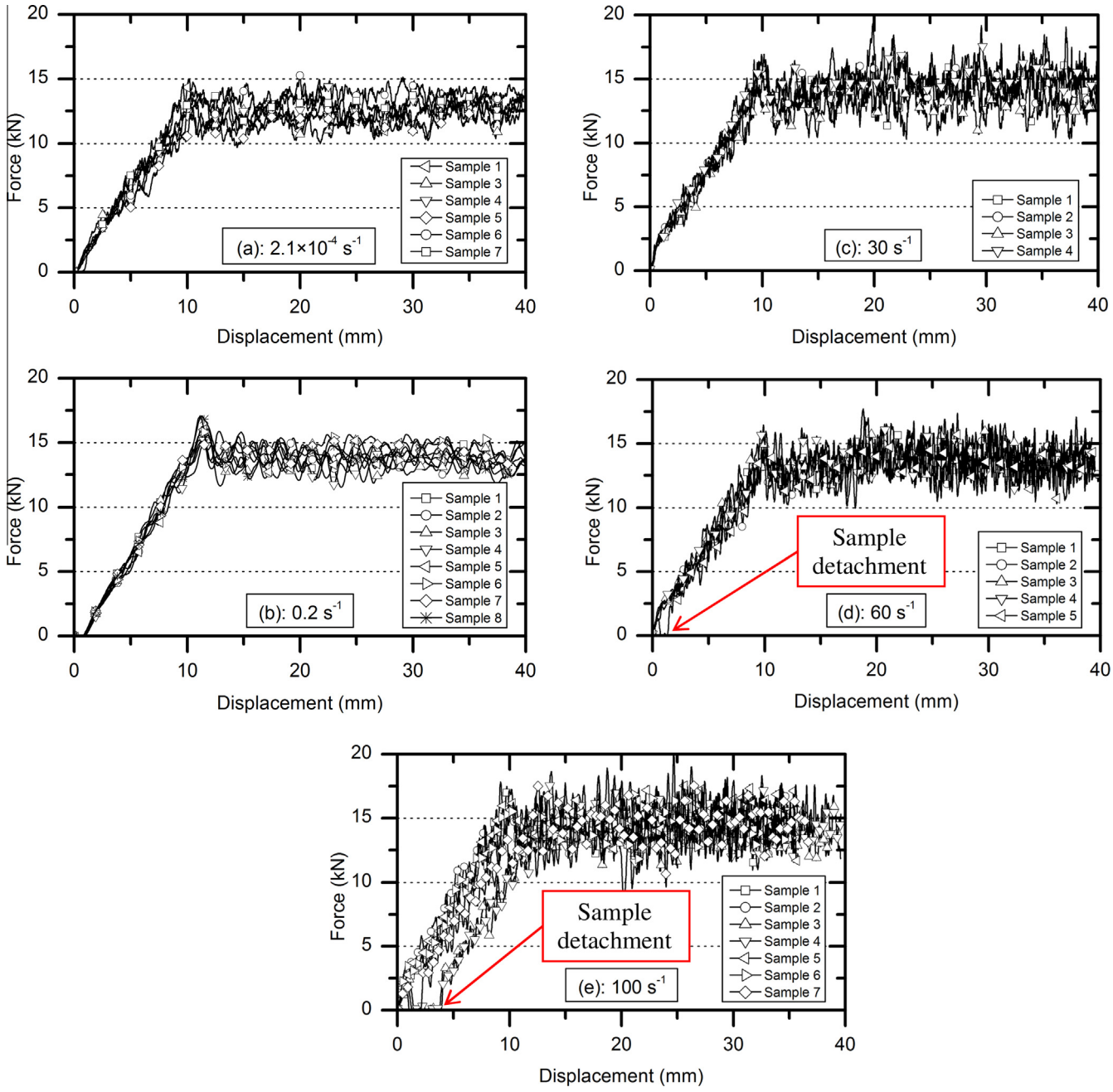

Fig. 7. Force response of specimens loaded at (a) 2.1×10^{-4}, (b) 0.2, (c) 30, (d) 60 and (e) 100 s^{-1}, with initial specimen detachment evident in (d) and (e).

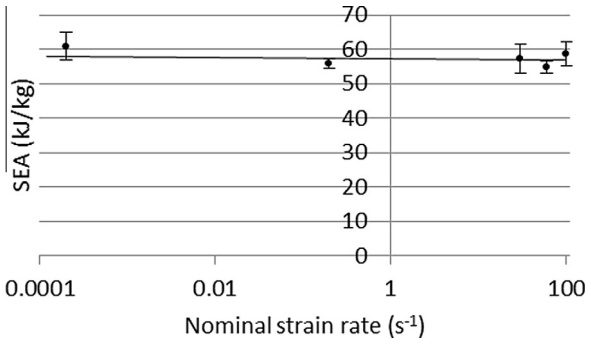

Fig. 8. Averaged SEA at different strain rates.

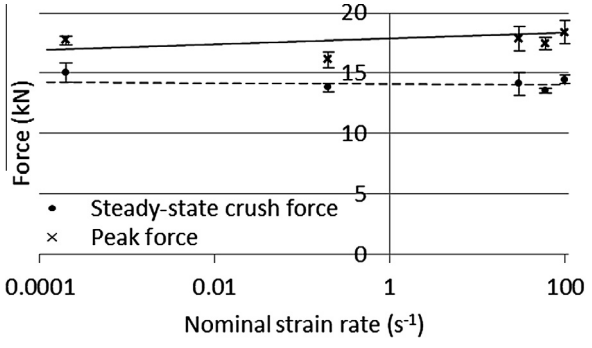

Fig. 9. Averaged peak (solid line) and steady-state crush load (dashed line) at different strain rates.

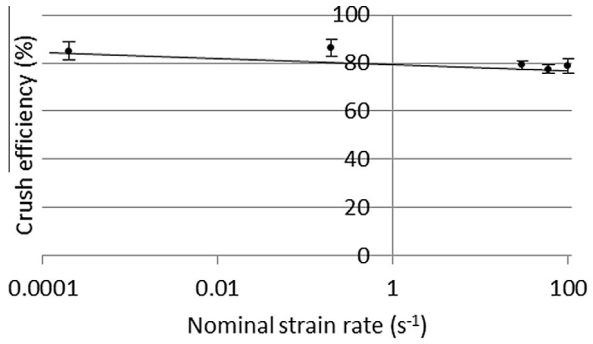

Fig. 10. Averaged crush efficiency at different strain rates.

Table 2
Results of linear regression performed on calculated metrics.

	SEA	F_{peak}	F_{SS}	*CE*
Regression gradient	−0.0092	0.0151	−0.0008	−0.0008
Std. error in gradient	0.0317	0.0041	0.0034	0.0002
Change over 100 s^{-1}	2.6%	9.0%	0.6%	8.9%

that the ply configuration is the cause of the apparent rate independence observed in this study.

While the literature is in disagreement over the effect of strain rate on the material response of composite materials [32], there have been suggestions that rate dependent phenomenon is driven by the polymer matrix phase of the composite laminate [33]. Koerber et al. [34] showed rate dependence in the matrix-dominated material properties beyond 200 s^{-1} and rate independence in fibre-dominated longitudinal compressive modulus [35] for a carbon–epoxy material system similar to the one used in this study. The observed rate insensitivity in the present study can be accounted for if rate effects are driven by the matrix material. T700/M21 prepreg has a relatively high fibre volume fraction due to its unidirectional nature. Hence the overall properties of the $[0/90/0/90]_s$ laminate are dominated by the fibre properties, minimising rate dependent effects on the averaged properties of the laminate. Furthermore, the transverse and shear stiffness, strengths as well as the critical energy release rates are all significantly lower than those in the longitudinal direction. The fibre-dominated critical energy release rates are 108 N/mm and 58.4 N/mm in tension and compression, respectively, in contrast to the 0.331 N/mm and 1.1 N/mm for transverse tension and compression as well as 0.443 N/mm in shear [36]. As the laminate was composed of equal amounts of 0° and 90° plies, the bulk of the energy absorption will be attributed to the fibre-dominated failure mode for a given volume of laminate crushed. A change in matrix-dominated energy release rate will have a relatively small effect on the overall energy absorption capability of the laminate. As a result, for fibre dominated layups, such as the one used in this study, strain rate dependence can be neglected.

4.3. Implications for analysis of energy absorber design

This result potentially has substantial impact on the design of composite energy absorbers. For materials configured like the T700/M21 cross ply laminate, the fibre-dominated nature of the material response allows strain rate dependence to be neglected. Jacob et al. [24] has identified that an increase in the amount of fibre fracture leads to increased energy absorption. Therefore, optimising the crush performance of a structure in the presence of a weight constraint would lead to the fibre-dominated damage mechanism being the dominant mode of energy absorption. The present results suggest that for these structures, strain rate independence can be assumed.

By discounting strain rate effect, the analysis of energy absorbing structures can be significantly simplified. When rate independence can be assumed, dynamic material properties, which are typically difficult to obtain and require specialised equipment such as the split Hopkinson bar or a hydraulic press, will not be needed. The analysis can also be conducted with rate independent constitutive equations, reducing the complexity and computational resources. Time scaling, which is a common method to speed up numerical solutions, can be used when the material response is rate independent.

5. Conclusions

The response of a tulip-triggered cylindrical energy absorbing structure undergoing crushing at increasing strain rates was investigated. The damage mechanisms have been identified from post-test inspections. The recorded force response was used to calculate the specific energy absorption (SEA), peak and steady-state forces as well as the crush efficiency.

A high level of consistency was achieved in the present study, indicating good reliability of the results. The observed fracture and damage distribution were indistinguishable between samples tested under the same conditions. Similarly, the standard

Fig. 11. Typical specimens from the 2.1×10^{-4} s^{-1} test.

deviations for the calculated metrics were small. The identified damage modes also correspond well with the literature.

Results indicate that the tested material is strain rate independent up to a strain rate of 100 s^{-1}. Damage modes and responses were found to be invariant with increasing loading rate experienced by the specimen. Analysis of the specific energy absorption and the steady-state crush force show them to be independent of applied strain rate. Changes in the peak force and the crush efficiency can be attributed to the experimental method rather than a change in the material behaviour. This rate independence is likely the result of a combination of the high fibre content of the laminate and the high fibre-dominated fracture energy release rates in comparison to those of matrix-dominated fracture in the material system used in this study.

For similar fibre-dominated material configurations, the strain rate dependence can be neglected. This speeds up the analysis process of composite energy absorbing structures by reducing the amount of material property data required for input, allowing the analysis to be performed with quasi-static assumptions and allowing for the use of time scaling in numerical models.

Acknowledgement

This work was undertaken within the Systems for Crashworthiness project, part of a CRC-ACS research program, established and supported under the Australian Government's Cooperative Research Centres Program. Prof Brian G. Falzon acknowledges the financial support of Bombardier and the Royal Academy of Engineering.

References

[1] JSSG-2010-7. Department of defense joint service specification guide – crew systems crash protection handbook. US Department of Defence; 2002.
[2] MIL-STD-1290A(AV). military standard light fixed and totary-wing aircraft crash resistance. US Department of Defence; 1988.
[3] Falzon BG, Apruzzese P. Numerical analysis of intralaminar failure mechanisms in composite structures. Part I: FE implementation. Compos Struct 2011;93:1039–46.
[4] Falzon BG, Apruzzese P. Numerical analysis of intralaminar failure mechanisms in composite structures. Part II: applications. Compos Struct 2011;93:1047–53.
[5] Tan W, Falzon BG, Price M. Predicting the crushing behaviour of composite material using high-fidelity finite element modelling. Int J Crashworthiness 2014:1–18.
[6] Jackson KE, Kellas S, Annett MS, Littell JD, Polanco MA. A comparative evaluation of two helicopter crash tests. In: 6th Fire and Cabin Safety Conference. Atlantic City, New Jersey: October 25–28, 2010; 2010.
[7] Palanivelu S, Van Paepegem W, Degrieck J, Van Ackeren J, Kakogiannis D, Van Hemelrijck D, et al. Experimental study on the axial crushing behaviour of pultruded composite tubes. Polym Test 2010;29:224–34.
[8] Thornton PH. Energy absorption in composite structures. J Compos Mater 1979;13:247–62.
[9] Farley GL. Energy absorption of composite materials. J Compos Mater 1983;17:267–79.
[10] Farley GL. The effects of crushing speed on the energy-absorption capability of composite tubes. J Compos Mater 1991;25:1314–29.
[11] Elgalai AM, Mahdi E, Hamouda AMS, Sahari BS. Crushing response of composite corrugated tubes to quasi-static axial loading. Compos Struct 2004;66:665–71.
[12] Kakogiannis D, Chung Kim Yuen S, Palanivelu S, Van Hemelrijck D, Van Paepegem W, Wastiels J, et al. Response of pultruded composite tubes subjected to dynamic and impulsive axial loading. Compos Part B: Eng 2013;55:537–47.
[13] Feraboli P, Wade B, Deleo F, Rassaian M. Crush energy absorption of composite channel section specimens. Compos Part A: Appl Sci Manuf 2009;40:1248–56.
[14] Ghasemnejad H, Blackman BRK, Hadavinia H, Sudall B. Experimental studies on fracture characterisation and energy absorption of GFRP composite box structures. Compos Struct 2009;88:253–61.
[15] Jiménez MA, Miravete A, Larrodé E, Revuelta D. Effect of trigger geometry on energy absorption in composite profiles. Compos Struct 2000;48:107–11.
[16] Mamalis AG, Manolakos DE, Ioannidis MB, Papapostolou DP. On the experimental investigation of crash energy absorption in laminate splaying collapse mode of FRP tubular components. Compos Struct 2005;70:413–29.
[17] Jackson A, Dutton S, Gunnion AJ, Kelly D. Investigation into laminate design of open carbon–fibre/epoxy sections by quasi–static and dynamic crushing. Compos Struct 2011;93:2646–54.
[18] David M, Johnson A, Voggenreiter H. Analysis of crushing response of composite crashworthy structures. Appl Compos Mater 2013;20:773–87.
[19] Garner DM, Adams DO. Test methods for composites crashworthiness: a review. J Adv Mater 2008;40:5–26.
[20] Palanivelu S, Paepegem WV, Degrieck J, Vantomme J, Kakogiannis D, Ackeren JV, et al. Crushing and energy absorption performance of different geometrical shapes of small-scale glass/polyester composite tubes under quasi-static loading conditions. Compos Struct 2011;93:992–1007.
[21] Joosten MW. Experimental and numerical investigation of triggered composite energy absorbing structures. University of New South Wales, Sydney, NSW, 2052, Australia: University of New South Wales; 2011.
[22] Pitarresi G, Carruthers JJ, Robinson AM, Torre G, Kenny JM, Ingleton S, et al. A comparative evaluation of crashworthy composite sandwich structures. Compos Struct 2007;78:34–44.
[23] Han H, Taheri F, Pegg N. Crushing behaviors and energy absorption efficiency of hybrid pultruded and ±45° braided tubes. Mech Adv Mater Struct 2011;18:287–300.
[24] Jacob GC, Fellers JF, Simunovic S, Starbuck JM. Energy absorption in polymer composites for automotive crashworthiness. J Compos Mater 2002;36:813–50.
[25] Mamalis AG, Manolakos DE, Ioannidis MB, Papapostolou DP. On the response of thin-walled CFRP composite tubular components subjected to static and dynamic axial compressive loading: experimental. Compos Struct 2005;69:407–20.
[26] Brighton A, Forrest M, Starbuck M, Erdman D, Fox B. Strain rate effects on the energy absorption of rapidly manufactured composite tubes. J Compos Mater 2009;43:2183–200.
[27] Huang J, Wang X. On a new crush trigger for energy absorption of composite tubes. Int J Crashworthiness. 2010;15:625–34.
[28] Jackson KE, Fuchs YT, Kellas S. Overview of the National Aeronautics and Space Administration Subsonic rotary wing aeronautics research program in rotorcraft crashworthiness. J Aerosp Eng 2009;22:229–39.
[29] Feraboli P. Current efforts in standardization of composite materials testing for crashworthiness and energy absorption. 47th AIAA/ASME/ASCE/AHS/ASC Structures, Structural Dynamics and Materials Conference, May 1, 2006 - May 4, 2006. Newport, RI, United states: American Institute of Aeronautics and Astronautics Inc., source: http://www.learningace.com/doc/1738707/c018105c74ba9f82f93ef4da2cee4895/aiaa-2006-2217-crush-mil17; 2006. p. 7427-44.
[30] Feraboli P. Development of a corrugated test specimen for composite materials energy absorption. J Compos Mater 2008;42:229–56.
[31] Berthe J, Brieu M, Deletombe E, Portemont G, Lecomte-Grosbras P, Deudon A. Consistent Identification of CFRP viscoelastic models from creep to dynamic loadings. Strain 2013;49:257–66.
[32] Jacob GC, Starbuck JM, Fellers JF, Simunovic S, Boeman RG. Strain rate effects on the mechanical properties of polymer composite materials. J Appl Polym Sci 2004;94:296–301.
[33] Jacob GC, Starbuck JM, Fellers JF, Simunovic S, Boeman RG. The effect of loading rate on the fracture toughness of fiber reinforced polymer composites. J Appl Polym Sci 2005;96:899–904.
[34] Koerber H, Xavier J, Camanho PP. High strain rate characterisation of unidirectional carbon–epoxy IM7-8552 in transverse compression and in-plane shear using digital image correlation. Mech Mater 2010;42:1004–19.
[35] Koerber H, Camanho PP. High strain rate characterisation of unidirectional carbon–epoxy IM7-8552 in longitudinal compression. Compos Part A: Appl Sci Manuf 2011;42:462–70.
[36] Falzon BG, Hawkins SC, Huynh CP, Radjef R, Brown C. An investigation of Mode I and Mode II fracture toughness enhancement using aligned carbon nanotubes forests at the crack interface. Compos Struct 2013;106:65–73.